IEEE Access
Multidisciplinary | Rapid Review | Open Access Journal

Received December 30, 2018, accepted January 18, 2019, date of publication January 31, 2019, date of current version February 20, 2019.

Digital Object Identifier 10.1109/ACCESS.2019.2895368

Joint Coding and Adaptive Image Transmission Scheme Based on DP-LDPC Codes for IoT Scenarios

LI DENG[1,2], ZHIPING SHI[1], (Member, IEEE), OUXUN LI[2,3], AND JIANBO JI[2]

[1]National Key Laboratory of Science and Technology on Communications, University of Electronic Science and Technology of China, Chengdu 611731, China
[2]School of Electronic Information and Automation, Guilin University of Aerospace Technology, Guilin 541004, China
[3]College of Automation Engineering, Nanjing University of Aeronautics and Astronautics, Nanjing 211106, China

Corresponding author: Zhiping Shi (szp@uestc.edu.cn)

This work was supported in part by the Natural Science Foundation of China under Grant 61671128, and in part by the Guangxi Natural Science Foundation under Grant 2018GXNSFAA281161.

ABSTRACT For wireless image communication in the Internet of Things (IoT) scenarios, fast and low error coding and transmission mechanisms are imperative. The joint source-channel coding scheme based on the double protograph low-density parity-check (DP-LDPC) codes would be a potential candidate due to the low complexity and good error performance. However, the error floor performance of DP-LDPC codes may deteriorate for source sequences with higher source probabilities or shorter block lengths. This paper aims to improve the traditional DP-LDPC image transmission system for the IoT scenarios from the following aspects. First, a joint optimization method of finite-length DP-LDPC codes is proposed to reduce the error floor while keeping satisfactory waterfall region performance. Second, an improved rate allocation strategy based on the fuzzy logic control is adopted to further improve the transmission reliability of the proposed short block length DP-LDPC codes. This scheme may offer some new solutions for the IoT image communication. The simulation results indicate the effectiveness of the proposed methods.

INDEX TERMS DP-LDPC codes, IoT image communication, JSCC, joint optimization, rate allocation.

I. INTRODUCTION

The Internet of Things (IoT) is the network of ''thing'', which is consist of the network connectivity, sensors, electronics, and software [1]. It is estimated that in 2020 about 14 billions devices will be connected in the IoT and applied for various scenarios [2]. For instance, in the Industrial Internet of Things (IIoT), many interesting applications such as the industrial equipment monitoring, the industrial property management, the smart factory and so on have received extensive concerns [3]. In the communication of IoT nodes (e.g., cameras, mobile devices, social media, the Internet), multimedia data, especially images would be the predominant form of transmitted data [4]. Advanced coding and transmission technologies are much needed for real time and reliable image communication. In the standardization of Narrow-band Internet of Things (NB-IoT) in Release 13, to reduce the user equipment complexity, all the down link channels use the Long Term Evolution (LTE) tail-biting convolutional code (TBCC); and the uplink shared channel uses the LTE turbo code for error correction [5]. Some advanced coding methods are also proposed for various IoT applications. The Low Density Generator Matrix (LDGM) based Raptor codes are proposed in [6] for Single Carrier Internet of Things (SC-IoT) to reduce the error floor with simple encoder and decoder. An image encoding and reconstruction scheme based on Reed Solomon (RS) codes is proposed to meet the need of low error transmission [7]. RS codes are also used for enhancing security in IoT based home automation for error detection and correction [8].

Compared with the convolutional codes, the short block length LDPC codes have similar decoding complexity and better error performance despite of the relative higher encoding complexity and decoding space complexity. Moreover, LDPC codes can be decoded completely in parallel, which makes short block length LDPC codes have certain advantages in communication systems with high performance and real-time requirements [**?**]. On the other hand, compared with the separate coding design, the joint source-channel coding (JSCC) has lower complexity and higher fidelity for

The associate editor coordinating the review of this manuscript and approving it for publication was Zhaoqing Pan.

2169-3536 © 2019 IEEE. Translations and content mining are permitted for academic research only.
Personal use is also permitted, but republication/redistribution requires IEEE permission.
See http://www.ieee.org/publications_standards/publications/rights/index.html for more information.

non-asymptotic and low latency scenarios, which is more suitable for resource-constrained, real time and time-varying communications, such as wireless image or video transmission [10]. In view of this, the JSCC scheme based on short block length LDPC codes are considered for IoT image communication in this paper.

JSCC schemes can be divided into two classes according to the way of source coding. One is the joint source-channel (JSC) decoding for the source with known coding formats (such as JPEG, JPEG2000, etc.) using channel decoders; the decoding performance of these schemes is greatly affected by the source encoder [11]. The other is the JSC decoding using the Tanner graphs of channel codes with known source statistical characteristics, which has lower system complexity. Among the second class of schemes, the double low-density parity-check codes (D-LDPC) proposed by Fresia, where LDPC codes are both used as the source code and the channel code, is widely used due to its good error performance [12]. The protograph LDPC codes (P-LDPC) are also introduced into the D-LDPC scheme to further reduce the system complexity and error floor performance, which is referred to as DP-LDPC codes [13]. Moreover, the radiography image transmission schemes based on DP-LDPC codes have also been employed for good image quality in bad channel conditions [14]–[16].

However, both D-LDPC codes and DP-LDPC codes suffer from the high error floor for source sequences with finite block length [12], [13]. In addition to the solutions of enlarging the block length or increasing the source coding rate, researches on the code design show the effectiveness on the error floor degradation. Thereinto, Beltrão Neto and Henkel [17] and Hong *et al.* [18] severally introduce a *linking matrix* into D-LDPC codes and DP-LDPC codes. He *et al.* [13] increase the degree of source check nodes while keeping the channel code fixed. On the other hand, two kinds of protogragh extrinsic information transfer algorithms (PEXIT) are presented for better analysis of DP-LDPC codes. One named as PEXIT-S [19] is used to analyze the source decoding threshold which represents the maximum compressible entropy of source codes with asymptotic block length; the other, called as PEXIT-D is presented to predict the system performance in waterfall region [20]. Chen *et al.* [21] use PEXIT-S to design the source code of DP-LDPC system with higher source decoding threshold and better error floor performance. In [22], a joint optimization method of DP-LDPC codes is proposed to search for the optimal code pair with the lowest decoding threshold for (asymptotically) long codewords; and a modified PEXIT with *length-N decoding threshold* is introduced to mitigate the finite length effect of short-to-moderate-length codewords.

For DP-LDPC image transmission system, error performance can also be improved by transmission strategies. In [14] and [15], source sequences are classified as low entropy frames (LEF) and high entropy frames (HEF). The LEF are coded by DP-LDPC codes, but the HEF are only coded by the channel encoder without source coding. Two different transmission architectures in one scheme inevitably increase the system complexity; and only channel coding for HEF would result in the efficiency reduction. In [16], image pre-processing is adopted before joint source-channel coding. The HEF are divided into sub-frames and filled up by zeros repeatedly until the source probability of all sub-frames are smaller than a certain threshold. At the receiver, frames are reconstructed by zeros deleting and sub-frames recombining. This pre-processing method burdens the system with additional data and processing time. In our previous work, a fuzzy logic control (FLC) based rate allocation method is proposed for better balance on the transmission efficiency, the image quality and the fairness of allocation [23]. Notice that, the frame lengths of all the mentioned image transmission schemes are longer than 2000 bits, which would lead to larger coding and decoding delay and is not suitable for real time communication.

This paper aims to improve the DP-LDPC based image transmission scheme to meet the needs of fast and low error communication in IoT scenarios. The technical difficulty lies in the design of short block length DP-LDPC codes with good error floor performance. First, an improved PEXIT-S algorithm for finite length codewords is proposed to better analyze the error floor performance of short block length DP-LDPC codes. Second, considering the optimization of source codes or the linking matrix for error floor reduction would result in the degradation of waterfall region performance [13], [18], a cascaded source-channel joint optimization method is proposed to trade off the performance on these two aspects. finally, to further improve the transmission reliability of the proposed short block length DP-LDPC codes, an improved FLC based rate allocation strategy is adopted to allocate the source coding rate and the channel coding rate according to the source probability and the channel condition. In summary, this paper improves the DP-LDPC image transmission system for IoT scenarios with the following contributions:

i) A stepwise joint optimization method of DP-LDPC codes is proposed to reduce the error floor of finite-length codewords on the premise of keeping satisfactory waterfall region performance.

ii) An improved fuzzy logic control (FLC) based rate allocation scheme is adopted to further improve the transmission reliability of short block length DP-LDPC codes.

The paper is organized as follows. The system description is presented in Section II. The detailed descriptions of the proposed methods are arranged in Section III. In Section IV, simulation and discussion are provided. The last part gives the summary. The list of acronyms used in this paper is shown in Table 1.

II. SYSTEM DESCRIPTION

A. SYSTEM MODEL

The system model of the proposed image transmission scheme based on DP-LDPC codes is shown in Fig.1. On the

TABLE 1. List of acronyms used in this paper.

acronyms	descriptions
ARA	accumulate-repeat-accumulate
AR4JA	accumulate-repeat-by-4-jagged-accumulate
AWGN	additive white Gaussian noise
BER	bit error rate
BP	belief propagation
BPSK	binary-phase-shift-keying
CNs	check nodes
DCT	discrete cosine transfrom
DE	differential evolution
D-LDPC	double low-density parity-check
DP-LDPC	double protograph low-density parity-check
FLC	fuzzy logic control
FPEXIT-S	finite-length protograph extrinsic information transfer for the source decoding threshold
GA	genetic algorithm
HEF	high entropy frames
HF	high frequency
IIoT	industrial Internet of Things
IoT	Internet of Things
JSC / JSCC	joint source-channel / joint source-channel coding
LDGM	low density generator matrix
LEF	low entropy frames
LF	low frequency
LLR	log-likelihood-ratio
LTE	Long Term Evolution
MI	mutual information
NB-IoT	narrow-band Internet of Things
PEG	progressive edge-growth
PEXIT	protograph extrinsic information transfer
PEXIT-D	PEXIT for the channel decoding threshold
PEXIT-S	PEXIT for the source decoding threshold
PSNR	peak-signal-to-noise-ratio
RS	Reed Solomon
R4JA	repeat-by-4-jagged-accumulate
SC-IoT	single carrier Internet of Things
SNR	signal-to-noise-ratio
TBCC	tail-biting convolutional code
VNs	variable nodes

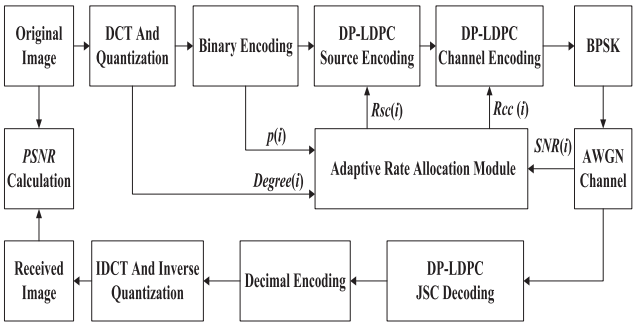

FIGURE 1. The system model of the image transmission scheme based on DP-LDPC codes.

sending side, the binarized discrete cosine transform (DCT) coefficients of the original image are successively encoded by the source encoder and the channel encoder. The source coding rate $R_{sc}(i)$ and the channel coding rate $R_{cc}(i)$ of the ith frame are calculated by the adaptive rate allocation module. The input parameters of this module are the source probability of the ith frame signed as $p(i)$, which denotes the probability of the binary bit "1" in the ith frame, the signal-to-noise-ratio (SNR) of the real-time channel denoted by $SNR(i)$, and the proportion of low frequency components in the ith frame represented as $Degree(i)$. After binary-phase-shift-keying (BPSK) modulation, the codeword is transmitted through the additive white Gaussian noise (AWGN) channel. At the receiving side, the received codeword is decoded by the JSC decoding. The peak-signal-to-noise-ratio (PSNR) of the received image is calculated for the quality evaluation.

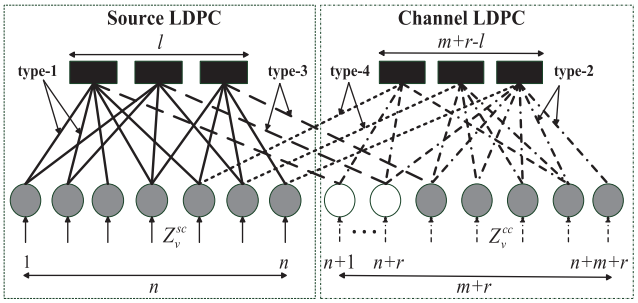

FIGURE 2. The Tanner graph of the DP-LDPC system.

B. ENCODING STRUCTURE

Fig.2 shows the Tanner graph of the DP-LDPC system [12], [13]. The left and right part represent the source code and the channel code, respectively. The black rectangles and gray circles denote the check nodes (CNs) and the variable nodes (VNs), respectively; and the white circles indicate the punctured channel VNs. This Tanner graph can be described by a joint base matrix $\mathbf{B}_J = (b_{i,j})$

$$\mathbf{B}_J = \begin{bmatrix} \mathbf{B}_{sc} & \mathbf{B}_{L1} \\ \mathbf{B}_{L2} & \mathbf{B}_{cc} \end{bmatrix}, \tag{1}$$

where the entry $b_{i,j}$ indicates the number of edges connecting CN_i and VN_j, $\mathbf{B}_{sc}$ is the source sub-matrix corresponding to type-1 edges (solid lines in Fig.2); $\mathbf{B}_{cc}$ is the channel sub-matrix corresponding to the type-2 edges (dash-dotted lines); $\mathbf{B}_{L1}$ describes the connections between each source CN and a single channel VN (type-3 edges, dashed lines); and $\mathbf{B}_{L2}$ represents the connections among each channel CN to a single source VN (type-4 edges, dotted lines). In this paper, $\mathbf{B}_{L1}$ follows the setting of [18] that the channel VNs with higher degrees are assigned to the source CNs; and the channel VNs with the highest degree are punctured. The joint parity-check matrix $\mathbf{H}_J$ can be generated by "copy-and-permute" on $\mathbf{B}_J$ [24]

$$\mathbf{H}_J = \begin{bmatrix} \mathbf{H}_{sc} & \mathbf{H}_{L1} \\ \mathbf{H}_{L2} & \mathbf{H}_{cc} \end{bmatrix}, \tag{2}$$

where $\mathbf{H}_{sc}$ is the $l \times n$ parity-check matrix of the source code, and $\mathbf{H}_{cc}$ is the parity-check matrix of the channel code with size of $(m + r - l) \times (m + r)$, where r is the number of punctured channel VNs. The source coding rate and the channel coding rates are calculated as $R_{sc} = l/n$, $R_{cc} = l/m$; the total transmission rate is $R = R_{cc}/R_{sc} = n/m$. The larger the total rate, the higher the transmission efficiency.

For schemes without type-4 edges [12], [13], $\mathbf{B}_{L2}$ and $\mathbf{H}_{L2}$ are zero matrices. Two cascaded LDPC codes perform source compression and channel coding, respectively. The codeword $\mathbf{c}$ is defined as $\mathbf{c} = \mathbf{u} \cdot \mathbf{G}_{cc} = \mathbf{s} \cdot \mathbf{H}_{sc}^{T} \cdot \mathbf{G}_{cc}$, where $\mathbf{s}$ is the source sequence, $\mathbf{u}$ is the compressed sequence, and $\mathbf{G}_{cc}$ is the corresponding generator matrix of $\mathbf{H}_{cc}$ [12]. For schemes with type-4 edges [17], the codeword $\mathbf{c}$ is defined as $\mathbf{c} = [\mathbf{s}, \mathbf{u}] \cdot \mathbf{G}_L = [\mathbf{s}, \mathbf{s} \cdot \mathbf{H}_{sc}^{T}] \cdot \mathbf{G}_L$, where $\mathbf{G}_L$ is the corresponding generator matrix of $\mathbf{H}_L = [\mathbf{H}_{L2}, \mathbf{H}_{cc}]$; and the first n bits of $\mathbf{c}$ need to be punctured before transmission. The former encoding scheme without type-4 edges is adopted and B_{L2} is a zero matrix in this paper. After BPSK modulation, the modulated codeword is denoted as $\mathbf{x} = 1 - 2\mathbf{c}$.

C. DECODING STRUCTURE

After transmitted through the AWGN channel, the received codeword $\mathbf{y}$ at the decoder can be expressed as $\mathbf{y} = \mathbf{x} + \mathbf{n}$, where $\mathbf{n} \sim \mathbf{N}(0, \sigma_{ch}^2)$, σ_{ch}^2 is the channel noise variance.

The decoding of DP-LDPC codes follows the procedure of belief propagation (BP) algorithm applied to the Tanner graph shown in Fig.2. The source decoder and the channel decoder run in parallel exchanging extrinsic information through the type-3 (and the type-4) edges. For independent binary sources transmitted over the AWGN channel, the log-likelihood-ratio (LLR) of source VNs is

$$Z_v^{sc} = \log((1-p)/p), \tag{3}$$

where p denotes the probability of the binary bit "1" in a source sequence, $v = 1, \ldots, n$; the LLR of channel VNs is

$$Z_v^{cc} = \begin{cases} 0, & \text{if it is a punctured VN} \\ 2y_v/\sigma_{ch}^2, & \text{otherwise} \end{cases} \tag{4}$$

where y_v is the vth symbol of transmitted codeword, $v = n+1, \ldots, n+m+r$. The entropy of a source sequence is defined as

$$H(s) = -p \cdot \log_2(p) - (1-p) \cdot \log_2(1-p). \tag{5}$$

The details of JSC decoding can be seen in [12] and [13].

III. DP-LDPC IMAGE TRANSMISSION SYSTEM

A. JOINT OPTIMIZATION OF DP-LDPC CODES

1) ROLE OF SOURCE CODES ON WATERFALL REGION PERFORMANCE

Due to the property that the same degree distribution may correspond to various protographs, the degree distribution based optimization methods of D-LDPC codes in [12] and [17] are not suitable for DP-LDPC codes. The joint PEXIT (PEXIT-D) is presented to predict the waterfall region performance of DP-LDPC codes [20]. In PEXIT-D, all the sub-matrices of $\mathbf{B}_J$ including $\mathbf{B}_{cc}$, $\mathbf{B}_{sc}$, $\mathbf{B}_{L1}$ and $\mathbf{B}_{L2}$ are involved with the mutual information (MI) update. Moreover, the MI between a posterior LLR evaluated by the source VN and the corresponding source bit is closely related to $\mathbf{B}_{sc}$. Beltrão Neto and Henkel [17] summarize the MI evolution for the source code in LDPC-based JSCC system as a function of the degree distribution of type-1 edges and type-2 edges $(\underline{\lambda}, \underline{d_c})$, the MI in the previous iteration of $l-1$, the source statistic characteristics p, and the channel condition σ_{ch}:

$$I_{v,l}^{(1)} = F_1(\underline{\lambda}, \underline{d_c}, I_{v,l-1}^{(1)}, p, \sigma_{ch}), \tag{6}$$

where $I_{v,l}^{(1)}$ is the MI between the messages sent through type-1 edges at the output of VNs at iteration l and the associated VN value,. For JSCC schemes without type-4 edges, the source VNs only have connections with type-1 edges. Therefore, $\mathbf{B}_{sc}$ is closely related to the waterfall region performance.

2) ROLE OF SOURCE CODES ON ERROR FLOOR PERFORMANCE

According to the lossless source coding theorem, for any stationary ergodic source sequence $\mathbf{s}$ and all $\epsilon > 0$, there exist fixed length compression codes with source coding rate R_{sc} exceeding the source entropy $H(s)$ plus ϵ with vanishing block error probability as the block length goes to infinity

$$R_{sc} > H(s) + \epsilon. \tag{7}$$

However, the finite length DP-LDPC codes suffer from high error floor when $H(s)$ approaches R_{sc}. The high bit error ratio (BER) residual is a consequence that the compressed source codeword forms error patterns that can not be corrected by the source LDPC codes [17], i.e., the error floor is due mainly to the source code [12]. For a source code with certain R_{sc}, the PEXIT-S algorithm can provide its source decoding threshold H_{th} (or the corresponding threshold of source probability p_{th}); and the satisfactory error floor performance can be achieved if the source sequence has $H(s)$ less than H_{th} and the block length approaches infinity.

$$H(s) < H_{th}. \tag{8}$$

Notice that, in the PEXIT-S algorithm, the channel decoding is assumed to be error free, i.e., the MI evolution is only determined by the source probability p and the source code. It is observed that the error floor performance can be improved by increasing the degree of source CNs [13], which can also be understood as to increase the entries of certain nodes in $\mathbf{B}_{sc}$, i.e., the number of type-1 edges. Similar with type-4 edges, the increase of type-1 edges can also improve the amount of available information about the source bits at the decoder. However, both the increase of the type-1 edges and the type-4 edges would shorten the girth of Tanner graph, i.e., the waterfall region performance might be lost to some extent [18].

3) IMPROVED PEXIT-S ALGORITHM FOR FINITE LENGTH CODEWORDS

The PEXIT-S algorithm is used for asymptotically long codewords, which may not be accurate for source sequences with finite block length. On the other hand, the MI in the $J_{BSC}(\cdot)$ function (see (9)) [12] of PEXIT-S algorithm is usually calculated by the Monte Carlo simulation, which would greatly

TABLE 2. Source decoding threshold (p_{th}) by PEXIT-S and FPEXIT-S.

code type	R_{sc}	PEXIT-S	FPEXIT-S $N = 9600$
R4JA code [25]	1/2	0.0850	0.0857
AR4JA code [25]	1/2	0.0950	0.0943
Non-precoded code [26]	1/2	0.0960	0.0959
$B_s^{1/2}$ [21]	1/2	0.0977	0.0971
Non-precoded code [26]	1/3	0.0502	0.0512
$B_s^{1/3}$ [21]	1/3	0.0519	0.0548
Non-precoded code [26]	1/4	0.0320	0.0319
$B_s^{1/4}$ [21]	1/4	0.0334	0.0369

TABLE 3. Source decoding threshold (p_{th}) by FPEXIT-S with different N.

code type	R_{sc}	FPEXIT-S $N = 9600$	FPEXIT-S $N = 3200$	FPEXIT-S $N = 400$
R4JA code [25]	1/2	0.0857	0.0820	0.0752
R4JA code [25]	1/3	0.0489	0.0459	0.0407
R4JA code [25]	1/4	0.0315	0.0295	0.0259

increase the time complexity of the code optimization.

$$J_{BSC}(\mu, p) = (1-p) \times I(V; \chi^{(1-p)}) + p \times I(V; \chi^{p}), \quad (9)$$

where $\mu = \sum_{s \neq j} b_{i,j}[J^{-1}(I_{Av}(s,j))]^2 + (b_{i,j} - 1)[J^{-1}(I_{Av}(i,j))]^2$, $I_{Av}(i,j)$ is the prior MI from VN_j to CN_i; $\chi^{(1-p)} \sim \mathbf{N}(\mu + L, 2\mu)$, $\chi^{p} \sim \mathbf{N}(\mu - L, 2\mu)$, L is the LLR of source VNs, and $I(V; \chi)$ denotes the MI between the source VN and χ.

In this paper, we improve the PEXIT-S for finite-length codewords and fast optimization, which is named as FPEXIT-S. The main modifications are listed as below:

i) The actual probability p' of a length-N sequence is used in FPEXIT-S, which approximately follows the Gaussian distribution $\mathbf{N}(p, p(1-p)/N)$ and is described as [22]

$$p' = p + \sqrt{p(1-p)/N} \cdot Q^{-1}(1-\beta), \quad (10)$$

where β is the confidence level that the actual probability lies below p', $\beta \in [0.5, 1]$, and $Q(x) = \frac{1}{\sqrt{2\pi}} \int_x^{\infty} e^{-\frac{t^2}{2}} dt$.

ii) The curve fitting method is used to calculate the MI in $J_{BSC}(\cdot)$ instead of the Monte Carlo simulation to reduce the computational complexity, which is described as

$$J'_{BSC}(\mu, p, N, \beta) \approx (1-p) \times J(\sqrt{\mu + e^{R_{sc}} \times (L')^2}) + p \times J(\sqrt{\mu - e^{R_{sc}} \times (L')^2}), \quad (11)$$

where $L' = \log((1-p')/p')$. Table 2 and Table 3 show the source decoding thresholds (the corresponding thresholds of source probabilities p_{th}) of some codes by PEXIT-S and FPEXIT-S. β is set as 0.99 in order to guarantee the convergence of PEXIT-D when N is 400; otherwise β is set as 0.9999. As shown in Table 2, when the block length is longer enough ($N = 9600$), the source decoding thresholds by FPEXIT-S are closely inosculate with those by PEXIT-S. In Table 3, As the block length gets shorter, the source decoding thresholds become smaller due to the worse finite-length effect.

4) SOURCE-CHANNEL JOINT OPTIMIZATION OF DP-LDPC CODES

Considering the dual role of source codes on the system performance in the error floor and the waterfall region, a stepwise source-channel joint optimization is proposed to guarantee the compromise performance between these two aspects. The general mechanism of the proposed method lies in that an allowable loss of waterfall region performance can be sacrificed to compensate the error floor performance.

We formulate the stepwise design as a cascaded optimization problem. First, $\mathbf{B}_{sc}$ and $\mathbf{B}_{cc}$ are jointly optimized for the optimal channel decoding threshold of DP-LDPC codes. The objective function of this step is defined as:

$$\textbf{step1} \qquad \min \theta(\mathbf{B}_J, p_{step1}) \quad (12)$$

$$\text{s.t.} \; f_1(\mathbf{B}_J, p_{step1}) = 1, \quad (13)$$

where the function $\theta(\mathbf{B}_J, p_{step1})$ returns the channel decoding threshold of $\mathbf{B}_J$ by PEXIT-D, $p_{step1} = \eta(\mathbf{B}_{sc\_orig}, N, \beta)$ is the source decoding threshold of the original source code by FPEXIT-S. Equation (13) represents the constraints of protograph design, which can be specified as

$$\begin{aligned} f_1(\mathbf{B}_J, p_{1\_step1}) = {} & (\theta(\mathbf{B}_J, p_{step1}) < \theta(\mathbf{B}_{J\_orig}, p_{step1})) \\ & \wedge (\theta(\mathbf{B}_{cc}, p_{step1}) < \theta(\mathbf{B}_{cc\_orig}, p_{step1})) \\ & \wedge (\delta(\mathbf{B}_{cc}) - \delta(\mathbf{B}_{cc\_orig}) > \alpha), \end{aligned} \quad (14)$$

where "$\wedge$" stands for the logical conjunction "and", $\mathbf{B}_{J\_orig}$ is the joint base matrix of the original DP-LDPC codes, where the source code and the channel code are R4JA and AR4JA codes [25], respectively, in this paper. $\mathbf{B}_{cc}$ and $\mathbf{B}_{cc\_orig}$ are the channel sub-matrices of $\mathbf{B}_J$ and $\mathbf{B}_{J\_orig}$, respectively. The function $\delta(\cdot)$ returns the typical minimum distance ratio of the channel code. The last two conditions in (14) are constraints to retain the good properties of state-of-the-art protograph LDPC codes on the channel decoding threshold and the minimum distance, respectively. α is an adjustable coefficient to constraint the performance loss of the minimum distance. The specific value of α is mainly determined by different requirements of the system performance, which is usually set as a negative number with smaller absolute value or a smaller positive number if better minimum distance performance is needed. Notice that the last constraint is invalid for codes without the property that the asymptotic ensemble minimum distance increases linearly with the block length, such as ARA codes [25].

Second, the source code of the optimal result in **step1** is further optimized for lower error floor performance with allowable performance loss of waterfall region. The objective function of this step is

$$\textbf{step2} \qquad \max p_{step2} = \eta(\mathbf{B}_{sc}, N, \beta) \quad (15)$$

$$\text{s.t.} \; f_2(\mathbf{B}_{sc}, p_{step2}) = 1, \quad (16)$$

where $p_{step2} = \eta(\mathbf{B}_{sc}, N, \beta)$ indicates the source decoding threshold of $\mathbf{B}_{sc}$ by FPEXIT-S; $f_2(\cdot)$ is described as

$$f_2(\mathbf{B}_{sc}, p_{step2}) = (\theta(\mathbf{B}_J, p_{step2}) < SNR_{max}) \wedge (\theta(\mathbf{B}_J, p_{step1}) - \theta(\mathbf{B}_{J\_orig}, p_{step1}) < SNR_{loss}), \tag{17}$$

where the two constraints in (17) are tradeoffs between the error floor and the waterfall region performance, SNR_{max} is the allowable maximum channel decoding threshold of optimal $\mathbf{B}_J$ in **step2** with p_{step2}, SNR_{loss} is the allowable maximum channel decoding threshold loss of optimal $\mathbf{B}_J$ in **step2** with p_{step1} compared with that of $\mathbf{B}_{J\_orig}$.

Considering the large search space of the joint base matrix, strategies based on the heuristic random search such as the differential evolution (DE) [21] and the genetic algorithm (GA) [22] are considered for the design of DP-LDPC codes with lower searching complexity. In this paper, GA combined with PEXIT analysis is adopted to search good codes in two cascaded optimization steps with subtle differences, which is described as follows:

GIVEN: The generation number g, the maximum generation number *Maxgen*, the population size *Num*, the crossover probability p_c, the mutation probability p_m, the maximum entry Max_{edge}, the base matrix to be optimized $\mathbf{B}_{int}$ and the set of fixed region $\mathbf{F}$ in $\mathbf{B}_{int}$ (i.e., the precoding structure, if applicable).

i) INITIALIZATION: let $g = 1$, $\mathbf{POP}_1^g = \mathbf{B}_{int}$, $\mathbf{B}_{best}^{g-1} = \mathbf{B}_{int}$, for $2 \le i \le Num$, $\mathbf{POP}_i^g$ is generated by randomly replacing one entry in each row of $\mathbf{POP}_1^g$ except region $\mathbf{F}$.

ii) CROSSOVER: for $i = 1 : 2 : Num$, $[s_1, s_2]$ denotes the size of $\mathbf{POP}_i^g$, the crossover proceeds with probability p_c and rand integers $r_1, r_2 \in [1, s_1 \times s_2]$, $r_1 < r_2$:

$$\begin{cases} \mathbf{C}_i^g(r_1 : r_2) & = \mathbf{POP}_{i+1}^g(r_1 : r_2) \\ \mathbf{C}_{i+1}^g(r_1 : r_2) & = \mathbf{POP}_i^g(r_1 : r_2) \end{cases} \tag{18}$$

iii) MUTATION: for $i = 1 : Num$, the mutation proceeds with probability p_m and rand integers $r_3, r_4 \in [1, s_1 \times s_2]$, $r_3 < r_4$:

$$\mathbf{M}_i^g(r_3 : r_4) = \mathbf{C}_i^g(r_4 : r_3) \tag{19}$$

iv) SELECTION: select the best individual $\mathbf{M}_{best}^g$ from $\mathbf{M}_i^g (1 \le i \le Num)$ according to the objective function of **step1** or **step2**, then update B_{best}^g:

$$\mathbf{B}_{best}^g = \begin{cases} \mathbf{M}_{best}^g & \text{if } \textbf{step1} \text{ or } \textbf{step2} \text{ is satisfied} \\ \mathbf{B}_{best}^{g-1} & \text{otherwise} \end{cases} \tag{20}$$

v) TERMINATION: if $g < Maxgen$, then $\mathbf{POP}^{g+1} = \mathbf{M}^g$, $g = g + 1$, returns to ii), otherwise output $\mathbf{B}_{best}^g$.

For the optimization of step 1, $\mathbf{B}_{int} = \mathbf{B}_{J\_orig}$. i) to iii) are executed separately for the source code and the channel code. Then, the two parts are combined as a new joint base matrix. Max_{edge} is set as the maximum value of entries in $\mathbf{B}_{J\_orig}$. For the optimization of **step2**, $\mathbf{B}_{int}$ is defined as the source code of the optimal result in **step1**; and the channel code of the optimal result in **step1** remains the same. Max_{edge} is set to be relatively larger than **step1** but not too big to avoid high encoding complexity.

B. FLC BASED RATE ALLOCATION SCHEME

1) CODING RATE SETS AND PROTOGRAPHS

In the rate allocation scheme, the candidates of R_{sc} and R_{cc} are severally included in the set of source coding rates $\mathfrak{R}_{sc}$ and the set of channel coding rates $\mathfrak{R}_{cc}$

$$\mathfrak{R}_{sc} = \left\{\frac{1}{4}, \frac{1}{3}, \frac{1}{2}, \frac{2}{3}, \frac{3}{4}, \frac{4}{5}\right\}, \tag{21}$$

$$\mathfrak{R}_{cc} = \left\{\frac{1}{5}, \frac{1}{4}, \frac{1}{3}, \frac{1}{2}, \frac{2}{3}\right\}, \tag{22}$$

where higher R_{sc} of 4/5 and lower R_{cc} of 1/5 are set for the source sequences with very high source probability and terrible channel condition, respectively. To guarantee the low error floor of short block length codewords, the channel coding rates higher than 2/3 are not included in $\mathfrak{R}_{cc}$.

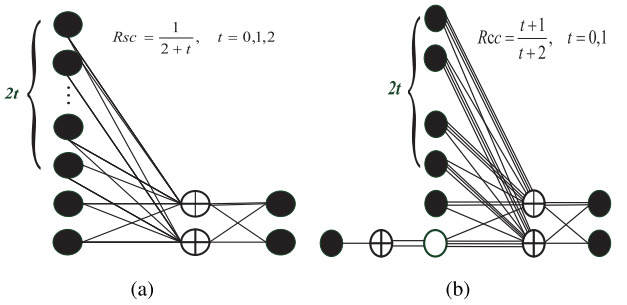

FIGURE 3. Protographs of the source code and the channel code: (a) Protographs of R4JA codes with R_{sc} of 1/2 and lower; (b) Protographs of AR4JA codes with R_{cc} of 1/2 and higher.

As $\mathbf{B}_{L1}$ and $\mathbf{B}_{L2}$ have fixed settings in the proposed method, the optimization of $\mathbf{B}_J$ is mainly for the code pair of ($\mathbf{B}_{sc}$, $\mathbf{B}_{cc}$). In this paper, the DP-LDPC codes are optimized based on ($\mathbf{B}_{R4JA}$, $\mathbf{B}_{AR4JA}$) code pairs. The protographs of R4JA codes with R_{sc} of 1/2 and lower are shown in Fig. 3(a); and the other higher rate codes are generated by the check node splitting technology in [25]. Fig. 3(b) shows the protographs of AR4JA codes with R_{cc} of 1/2 and higher; and the rest lower rate channel codes are made by the check matrix extension in [27]. All the base matrices of the proposed code pairs ($\mathbf{B}_{IR4JA}$, $\mathbf{B}_{IAR4JA}$) with rates in $\mathfrak{R}_{sc}$ and $\mathfrak{R}_{cc}$ are listed in the APPENDIX.

2) FLC BASED RATE ALLOCATION MODULE

The motivation of rate allocation in this paper is to ensure the transmission reliability by allocating R_{sc} and R_{cc} according to the source probability and the importance of each frame, addition with the real time channel condition. However, due to the differences of the source probability, the importance and the channel situation for each frame, deterministic methods based on accurate mathematical models are not suitable for rate allocation in this paper. Considering the good robustness

and low complexity, the fuzzy logic controller is adopted to adaptively allocate R_{sc} and R_{cc} for each frame. The major difference from the rate allocation scheme in [23] is that the transmission efficiency is sacrificed for high reliability and no longer the optimization object.

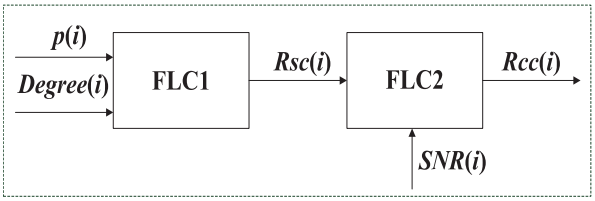

FIGURE 4. The block diagram of FLC based rate allocation module.

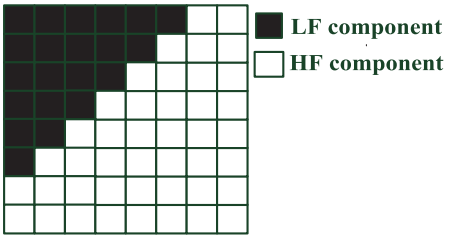

FIGURE 5. The frequency distribution in a 8 × 8 DCT block.

The diagram of FLC based rate allocation module is shown in Fig.4, which is cascaded by two fuzzy logic controllers FLC1 and FLC2. Both controllers have the same structure of double-input and single-output. The inputs of FLC1 include the source probability $p(i)$ and the importance factor $Degree(i)$ of the ith frame. Fig.5 shows the frequency distribution of a 8×8 DCT block. The black squares in top left corner represent the low frequency (LF) components, and the rest squares with white color denote the high frequency (HF) components. Considering the LF components include the key information of an image and are sensitive to noise, $Degree(i)$ is defined as the proportion of LF components in an image frame to measure its importance. Larger $Degree(i)$ indicates higher importance and more protection. $R_{sc}(i)$ is the output of FLC1 which is also the input of FLC2. The other input of FLC2 $SNR(i)$ is the SNR when transmitting the ith frame; and $R_{cc}(i)$ is the output of FLC2. The role of $R_{sc}(i)$ in FLC2 is adjusting $R_{cc}(i)$ to protect the frames with large source probabilities or high importance.

3) MEMBERSHIP FUNCTION CURVES

Fig.6 depicts the membership function curves of FLC1 and FLC2. As seen in Fig.6, the membership function curves are set as the types of trapezoid and triangle. The fuzzy domains of $R_{sc}(i)$ and $R_{cc}(i)$ are [0.2, 0.85] and [0.15, 0.75], respectively. The fuzzy domains of $p(i)$ and $Degree(i)$ are determined by the images to be transmitted, which are set as [0, 0.16] and [0, 0.8] in this paper. The range of $SNR(i)$ is set to be $[-1, 3]$dB.

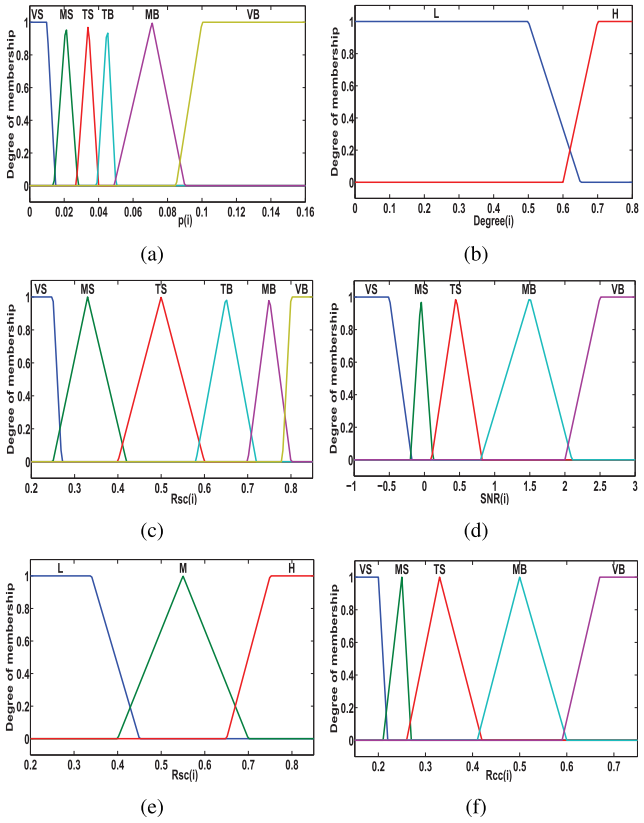

FIGURE 6. Membership function curves of the input and output variables in FLC1 and FLC2: (a) FLC1 input variable $p(i)$; (b) FLC1 input variable $Degree(i)$; (c) FLC1 output variable $Rsc(i)$; (d) FLC2 input variable $SNR(i)$; (e) FLC2 input variable $R_{sc}(i)$; (f) FLC2 output variable $R_{cc}(i)$.

The input $p(i)$ and the output $R_{sc}(i)$ in FLC1, addition with the input $SNR(i)$ and the output $R_{cc}(i)$ in FLC2 have the linguistic values of "Very Small", "Medium Small", "Tiny Small", "Tiny Big", "Medium Big" and "Very Big", which are signed as "VS", "MS", "TS", "TB", "MB" and "VB" for short; while the FLC1 input $Degree(i)$ and the FLC2 input $R_{sc}(i)$ have the linguistic values of "Low", "Medium" and "High" denoted by "L", "M" and "H".

The specific fuzzy domain of each linguistic value can be checked on the sub-image abscissas in Fig.6. It should be noted that the fuzzy domains of linguistic values of $R_{sc}(i)$ and $R_{cc}(i)$, which severally correspond to $p(i)$ and $SNR(i)$ with the same linguistic values, need to be higher and lower than the thresholds by FPEXIT-S and PEXIT-D, respectively. Considering the finite length of image frames, $R_{sc}(i)$ and $R_{cc}(i)$ are allocated separately higher and lower enough to guarantee the transmission reliability.

4) FUZZY LOGIC RULES

Table 4 and Table 5 list the fuzzy logic rules of FLC1 and FLC2, respectively, which are explained in detail as below.

Table 4 contains 12 rules in total. Rules 1 to 6 are set for frames with low importance, in which the value of $Degree(i)$ is "L". There is no protective measures in these 6 rules.

TABLE 4. The fuzzy logic rules of FLC1.

Variables	1	2	3	4	5	6	7	8	9	10	11	12
$p(i)$	VS	MS	TS	TB	MB	VB	VS	MS	TS	TB	MB	VB
$Degree(i)$	L	L	L	L	L	L	H	H	H	H	H	H
$R_{sc}(i)$	VS	MS	TS	TB	MB	VB	VS	MS	TB	MB	VB	VB

TABLE 5. The fuzzy logic rules of FLC2.

Variables	1	2	3	4	5	6	7	8
$SNR(i)$	VS	MS	TS	MB	VB	VS	MS	TS
$R_{sc}(i)$	L	L	L	L	L	M	M	M
$R_{cc}(i)$	VS	VS	MS	MB	VB	VS	VS	MS
Variables	9	10	11	12	13	14	15	
$SNR(i)$	MB	VB	VS	MS	TS	MB	VB	
$R_{sc}(i)$	M	M	H	H	H	H	H	
$R_{cc}(i)$	TS	MB	VS	VS	VS	TS	MB	

While in rules 7 to 12 with $Degree(i)$ of "H", higher values of $R_{sc}(i)$ are only allocated for frames with both larger $Degree(i)$ and higher $p(i)$. The reason it that most LF components in some frames are so small that might be quantified as zeros, which would result in low source probability of these frames. Higher $R_{sc}(i)$ indicates lower source compression ratio for these special frames.

Table 5 has totally 15 rules. In rules 1 to 5, the values of input $R_{sc}(i)$ are "L", which means the source has smaller $p(i)$, the values of output $R_{cc}(i)$ are set smaller only in low SNR region. In rules 6 to 10 and rules 11 to 15, $R_{sc}(i)$ are "M" and "H", respectively, indicating higher $p(i)$ or $Degree(i)$ of the ith frame. For these frames, protective measures are stronger than rules 1 to 5. The values of $R_{cc}(i)$ in high SNR region are also smaller than those in rules 3 to 5. Lower $R_{cc}(i)$ can protect the important frames or frames with high probabilities by stronger error resistance.

IV. SIMULATION AND DISCUSSION

In this section, two sets of experiments have been performed to validate the effectiveness of the proposed methods. In the first part, we show the superiority of the joint optimized codes over the code pairs with single optimized B_{sc} or B_{cc}; then we compare the proposed codes with the existing performance records; In the second part, we show the advantage of the proposed codes combined with the FLC based rate allocation scheme on the transmission reliability.

In the first experiment, the source sequence with short block length of $N = 400$ is considered to be encoded by the original code pair $(\mathbf{B}_{R4JA\_1/2}, \mathbf{B}_{AR4JA\_1/2})$ and the optimized code pair $(\mathbf{B}_{IR4JA\_1/2}, \mathbf{B}_{IAR4JA\_1/2})$ with $R_{sc} = 1/2$ and $R_{cc} = 1/2$; The corresponding sub-matrices are listed in (23) to (26). To demonstrate the roles of each sub-matrix on the waterfall region performance and the error floor performance, the code pairs of $(\mathbf{B}_{IR4JA\_1/2}, \mathbf{B}_{AR4JA\_1/2})$ and $(\mathbf{B}_{R4JA\_1/2}, \mathbf{B}_{IAR4JA\_1/2})$ are also involved in the comparison. The base matrices are lifted with the progressive edge-growth (PEG) algorithm [28]. The parameters of GA based optimization method are set as below: the crossover probability is $p_c = 0.8$, the mutation probability is $p_m = 0.2$, the population size is $Num = 50$, and the maximum generation number is $Maxgen = 100$, Max_{edge} in step 2 is set as 9, β in (10) is 0.99, α in (14) is set to be -0.01.

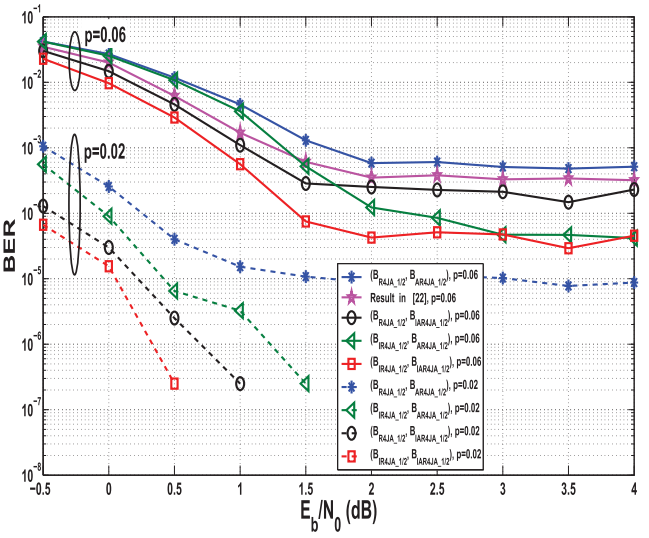

FIGURE 7. Comparison with optimization for different sub-matrices with $R_{sc} = 1/2$, $R_{cc} = 1/2$, $N = 400$, $p = 0.02$ and $p = 0.06$.

$$\mathbf{B}_{R4JA\_1/2} = \begin{bmatrix} 3 & 1 & 1 & 1 \\ 1 & 2 & 1 & 2 \end{bmatrix} \tag{23}$$

$$\mathbf{B}_{IR4JA\_1/2} = \begin{bmatrix} 3 & 1 & 1 & 2 \\ 6 & 1 & 1 & 1 \end{bmatrix} \tag{24}$$

$$\mathbf{B}_{AR4JA\_1/2} = \begin{bmatrix} 1 & 2 & 0 & 0 & 0 \\ 0 & 3 & 1 & 1 & 1 \\ 0 & 1 & 2 & 2 & 1 \end{bmatrix} \tag{25}$$

$$\mathbf{B}_{IAR4JA\_1/2} = \begin{bmatrix} 1 & 2 & 0 & 0 & 0 \\ 0 & 2 & 1 & 1 & 1 \\ 0 & 1 & 2 & 1 & 1 \end{bmatrix} \tag{26}$$

As shown in Fig.7, for source sequences with smaller probability of $p = 0.02$, the BER curve of $(\mathbf{B}_{R4JA\_1/2}, \mathbf{B}_{AR4JA\_1/2})$ code pair has lower error floor at the BER of 10^{-5}; the three other optimized code pairs can be free of error with different waterfall region performances. $(\mathbf{B}_{IR4JA\_1/2}, \mathbf{B}_{AR4JA\_1/2})$ with single optimized $\mathbf{B}_{sc}$ has 0.5dB coding gain loss at the BER of 2.5×10^{-7} compared to $(\mathbf{B}_{R4JA\_1/2}, \mathbf{B}_{IAR4JA\_1/2})$ with single optimized $\mathbf{B}_{cc}$; However, $(\mathbf{B}_{IR4JA\_1/2}, \mathbf{B}_{IAR4JA\_1/2})$ with joint optimized $\mathbf{B}_{sc}$ and $\mathbf{B}_{cc}$ can achieve 0.5dB coding gains over $(\mathbf{B}_{R4JA\_1/2}, \mathbf{B}_{IAR4JA\_1/2})$, which indicates the superiority of the joint optimization method on the waterfall region performance. On the other hand, for the source sequence with higher probability of $p = 0.06$, the BER curve of $(\mathbf{B}_{R4JA\_1/2}, \mathbf{B}_{AR4JA\_1/2})$ has a high error floor at 5×10^{-4}; the BER curves of $(\mathbf{B}_{IR4JA\_1/2}, \mathbf{B}_{AR4JA\_1/2})$ and $(\mathbf{B}_{R4JA\_1/2}, \mathbf{B}_{IAR4JA\_1/2})$ separately show a lower error floor at 4×10^{-5} and a better waterfall region about 0.75dB earlier than that of $(\mathbf{B}_{R4JA\_1/2}, \mathbf{B}_{AR4JA\_1/2})$ at the BER of 5×10^{-4}; while $(\mathbf{B}_{IR4JA\_1/2}, \mathbf{B}_{IAR4JA\_1/2})$ can both obtain a similar error

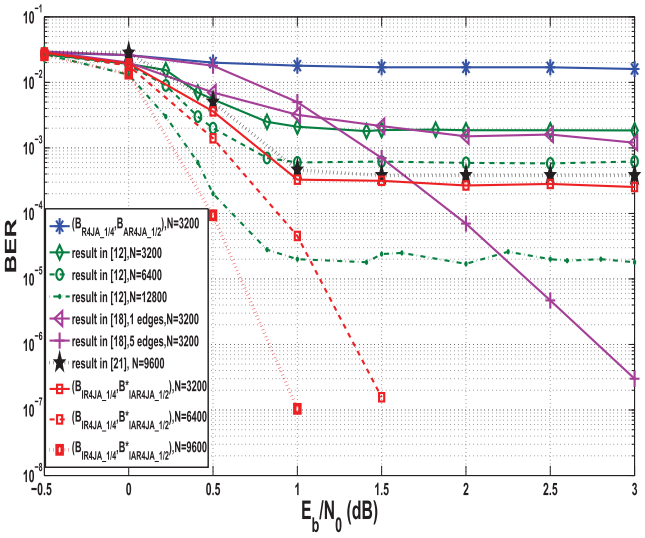

FIGURE 8. Comparison with existing performance records with $R_{sc} = 1/4$, $R_{cc} = 1/2$, $p = 0.03$.

floor with ($\mathbf{B}_{IR4JA\_1/2}$, $\mathbf{B}_{AR4JA\_1/2}$) and 1dB coding gains over ($\mathbf{B}_{R4JA\_1/2}$, $\mathbf{B}_{AR4JA\_1/2}$) at the BER of 5×10^{-4}. The existing performance record in [22] for the source sequence with $p = 0.06$ and $N = 400$ is also shown in Fig.7, which has a similar error floor with ($\mathbf{B}_{R4JA\_1/2}$, $\mathbf{B}_{IAR4JA\_1/2}$) at the BER about 3×10^{-4}.

Fig.8 shows the comparison with the existing performance records with $N = 3200$ and $p = 0.03$; the coding rates are $R_{sc} = 1/4$ and $R_{cc} = 1/2$; and the optimization parameter β is set to be 0.9999. The sub-matrices of ($\mathbf{B}_{R4JA\_1/4}$, $\mathbf{B}_{AR4JA\_1/2}$) are listed in (27) and (25); and the sub-matrices of the optimized code pair ($\mathbf{B}_{IR4JA\_1/4}$, $\mathbf{B}^*_{IAR4JA\_1/2}$) are listed in (28) and (29). According to PEXIT-S, $p = 0.03$ is a relative higher probability for DP-LDPC codes with $R_{sc} = 1/4$. Various methods are proposed to reduce the error floor, such as enlarging the code length [12], increasing the edges in sub-matrix B_{L2} [18], and optimizing the sub-matrix B_{sc} with asymptotic analysis [21]. As seen in Fig.8, the error floor of ($\mathbf{B}_{IR4JA\_1/4}$, $\mathbf{B}^*_{IAR4JA\_1/2}$) with $N = 3200$ is about 3×10^{-4} at 3dB, which is similar with that of the proposed codes in [12] with $N = 6400$ and the proposed codes in [21] with $N = 9600$. Moreover, the proposed code pair ($\mathbf{B}_{IR4JA\_1/4}$, $\mathbf{B}^*_{IAR4JA\_1/2}$) can be free of error at 1dB and 1.5dB with $N = 9600$ and $N = 6400$, respectively. The proposed codes in [18] with 5 edges connections in B_{L2} can also be no error floor at 3dB with significant gain loss in waterfall region. On the other hand, the proposed codes in [18] with 1 edge connection has little improvement on the error floor performance; and an appropriate number of edge connections should be considered for the compromise performance between the error floor and the waterfall region.

$$\mathbf{B}_{R4JA\_1/4} = \begin{bmatrix} 3 & 1 & 3 & 1 & 3 & 1 & 1 & 1 \\ 1 & 2 & 1 & 3 & 1 & 3 & 1 & 3 \end{bmatrix} \quad (27)$$

$$\mathbf{B}_{IR4JA\_1/4} = \begin{bmatrix} 1 & 1 & 8 & 3 & 3 & 3 & 2 & 2 \\ 1 & 1 & 9 & 1 & 2 & 3 & 1 & 1 \end{bmatrix} \quad (28)$$

$$\mathbf{B}^*_{IAR4JA\_1/2} = \begin{bmatrix} 1 & 2 & 0 & 0 & 0 \\ 0 & 2 & 1 & 1 & 1 \\ 0 & 1 & 3 & 1 & 1 \end{bmatrix} \quad (29)$$

In conclusion, for source sequences with higher probabilities and finite block lengths, the proposed codes can achieve lower error floor while keeping satisfactory waterfall region performance compared with the existing DP-LDPC codes.

In the second experiment, the FLC based rate allocation scheme combined with the optimized code pairs listed in the APPENDIX are used for the image transmission in the time-invariant channel and the time-varying channel. Three classical images of "Lena", "Peppers" and "X-ray" with size of 256×256 are selected for transmission; and their PSNR values after DCT transform and quantization are 34.2359dB, 33.8823dB and 36.1267dB, respectively. The short block length of $N = 720$ is adopted to meet the need of low-delay communication. For convenience of analysis, the methods in [16] is named as the pre method for short, where the frame splitting and zero filling technology is proposed to reduce the source probability and only a code pair of ($\mathbf{B}_{R4JA\_1/2}$, $\mathbf{B}_{AR4JA\_1/2}$) is adopted. The proposed FLC based rate allocation combined with ($\mathbf{B}_{R4JA}$, $\mathbf{B}_{AR4JA}$) code pairs is denoted as the pro1 method; and the FLC based rate allocation combined with the proposed code pairs ($\mathbf{B}_{IR4JA}$, $\mathbf{B}_{IAR4JA}$) is signed as the pro2 method.

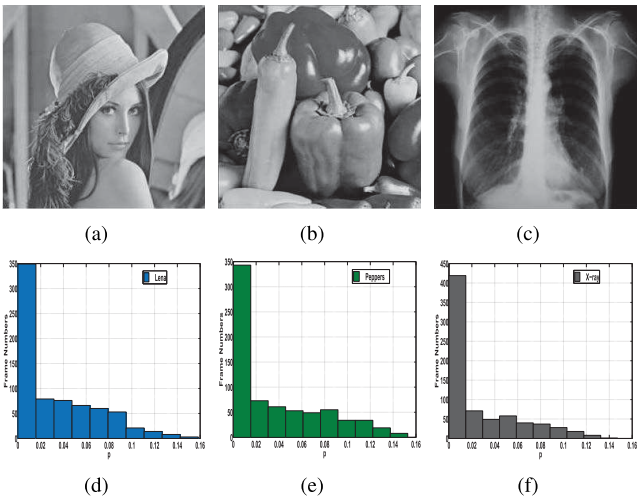

FIGURE 9. Original images and corresponding histograms of the source statistic characteristics: (a) Original "Lena"; (b) Original "Peppers"; (c)Original "X-ray"; (d) source probability histogram of "Lena"; (e) source probability histogram of "Peppers"; (f) source probability histogram of "X-ray".

Fig.9 shows the original images and corresponding histograms of the source statistic characteristics. The range of the source probability p is between 0 to 0.16. Among these images, "X-ray" has the highest proportion of frames with

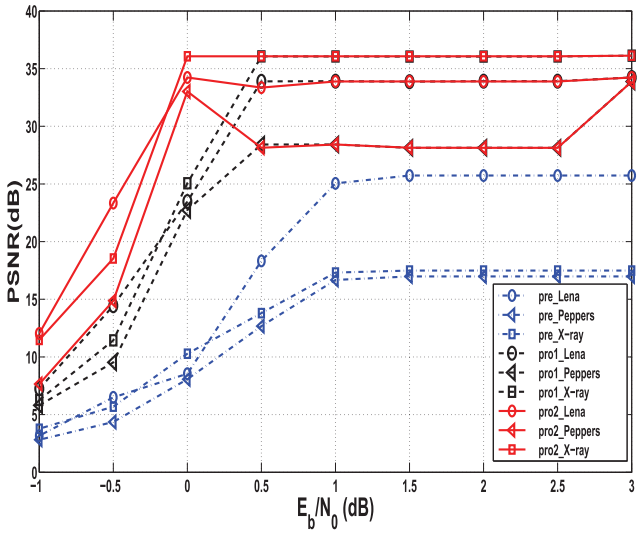

FIGURE 10. PSNR curves of received images in the time-invariant channel.

lower probabilities, while "Peppers" has the most frames with probabilities higher than 0.1.

Fig.10 gives the PSNR values of the received images in the time-invariant channel. As seen in Fig.10, in the bad channel condition with the SNR lower than 0dB, the pro2 method has the highest transmission quality. At the SNR of 0dB, compared with the pre method, the pro1 method achieves about 15dB transmission gains on PSNR by the rate allocation; and the pre2 method further attains about 10dB gains on PSNR by the code optimization. Both the pro1 method and the pro2 method can achieve high PSNR close to those of the original images at the SNR of 3dB. The PSNR values of the pre method are stable after the SNR of 1.5dB but lower than those of the original images at least 8.5dB.

TABLE 6. Transmission performances in the time-invariant channel (0dB).

Images	Methods	PSNR (dB)	R_mean	N_frames
Lena	pre	8.5472	1	897
Lena	pro1	23.4705	0.3249	729
Lena	pro2	34.2324	0.3249	729
Peppers	pre	8.0678	1	946
Peppers	pro1	22.7345	0.3231	729
Peppers	pro2	33.8823	0.3231	729
X-ray	pre	10.2765	1	852
X-ray	pro1	25.0615	0.2642	729
X-ray	pro2	36.0689	0.2642	729

Table 6 and Fig.11 show the transmission performance in the time-invariant channel with the SNR of 0dB. In Table 6, R_mean denotes the average transmission rate, and N_frames is the number of transmitted frames. In the pre method, R_mean has the fixed value of 1, while the values of R_mean in the pro1 and the pro2 method are much lower to compensate the transmission quality. The total frames transmitted by the pre1 method varies from images, the more the frames with higher probabilities, the larger the value of N_frames. As seen in Fig.11, considering only 1/2 R_{sc} and 1/2 R_{cc} are adopted

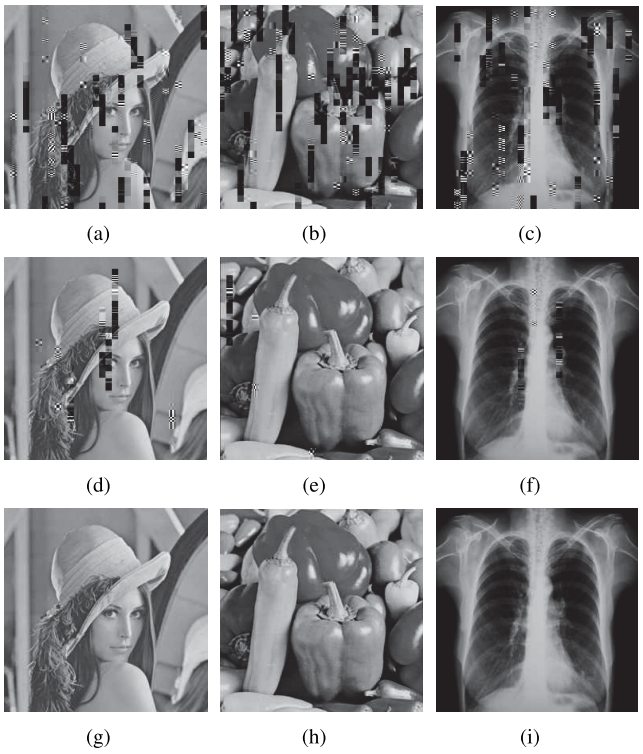

FIGURE 11. Received images in the time-invariant channel with $SNR = 0$ dB : (a) Received "lena" by pre; (b) Received "Peppers" by pre; (c) Received "X-ray" by pre; (d) Received "lena" by pro1; (e) Received "Peppers" by pro1; (f) Received "X-ray" by pro1; (g) Received "lena" by pro2; (h) Received "Peppers" by pro2; (i) Received "X-ray" by pro2.

TABLE 7. Transmission performances in the time-varying channel ([−1,3]dB).

Images	Methods	PSNR (dB)	R_mean	N_frames
Lena	pre	8.2494	1	897
Lena	pro1	17.6793	0.6105	729
Lena	pro2	29.3288	0.5977	729
Peppers	pre	8.1043	1	946
Peppers	pro1	13.2605	0.6061	729
Peppers	pro2	22.9713	0.6091	729
X-ray	pre	10.1036	1	852
X-ray	pro1	20.1505	0.4858	729
X-ray	pro2	31.3583	0.4874	729

in the pre method, the error performance is even worse in the low SNR region. Owing to the rate allocation and the optimized code pairs, the pro2 method has the best received image quality, which can transmit images with little error at the SNR of 0dB.

Comparisons in the time-varying channel are also provided. In this experiment, the channel condition randomly changes with frame in the range of [−1, 3] dB. As seen in Table 7 and Fig.12, the pre method cannot well adapt the real time channel condition, which has much lower transmission quality. In the pro1 method and the pro2 method, about 40% to 50% transmission efficiency is sacrificed for satisfactory image quality. However, successive error blocks still exist in the received images by the pro1 method. Owing to

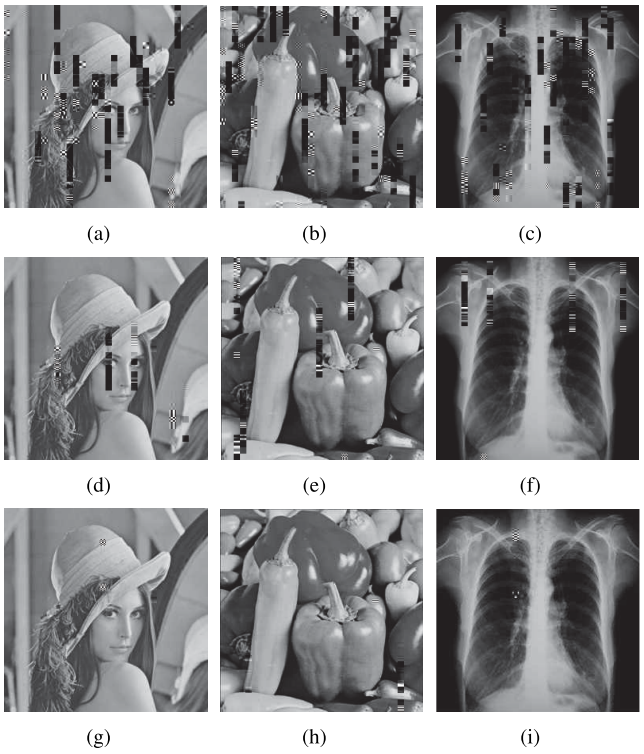

FIGURE 12. Received images in the time-varying channel ([−1,3] dB): (a) Received "lena" by pre; (b) Received "Peppers" by pre; (c) Received "X-ray" by pre; (d) Received "lena" by pro1; (e) Received "Peppers" by pro1; (f) Received "X-ray" by pro1; (g) Received "lena" by pro2; (h) Received "Peppers" by pro2; (i) Received "X-ray" by pro2.

the optimized codes, more transmission gains on PSNR are achieved by the pro2 method, which can transmit the images with satisfying vision while the channel varies from −1dB to 3dB. Due to the image "Peppers" contains the most frames with higher source probabilities, the PSNR values of the corresponding received images are relative lower than those of other images.

V. CONCLUSION

This paper aims to improve the DP-LDPC image transmission system for fast and low error communication in IoT scenarios. Joint optimization of finite length DP-LDPC codes and quality-oriented rate allocation scheme are proposed to guarantee the transmission reliability of the short block length DP-LDPC codes; and considerable transmission gains can be achieved from both aspects. However, improvements need to be developed in the future work. First, as shown in the APPENDIX, some code pairs with higher R_{sc} or lower R_{cc} have not the optimal results by GA based heuristic random search, thus the proposed optimization method needs to be further improved. Second, more practical channel models and corresponding design schemes will be further considered. Finally, we intend to apply the improved scheme for the medical image transmission in IIoT healthcare applications.

TABLE 8. Optimized code pairs with parameters of $N = 720$ and $\beta = 0.99$.

Types	B_{sc}	B_{cc}
$(\mathbf{B}_{sc\_1/4}, \mathbf{B}_{cc\_2/3})$	$\begin{pmatrix} 3\,1\,1\,3\,3\,1\,1\,1 \\ 1\,2\,1\,3\,3\,3\,3\,2 \end{pmatrix}$	$\begin{pmatrix} 1\,2\,0\,0\,0\,0\,0 \\ 0\,3\,3\,1\,1\,1\,1 \\ 0\,1\,1\,1\,1\,2\,2 \end{pmatrix}$
$(\mathbf{B}_{sc\_1/3}, \mathbf{B}_{cc\_2/3})$	$\begin{pmatrix} 1\,3\,2\,1\,1\,7 \\ 1\,1\,3\,1\,3\,2 \end{pmatrix}$	$\begin{pmatrix} 1\,2\,0\,0\,0\,0\,0 \\ 0\,3\,3\,1\,1\,1\,2 \\ 0\,1\,2\,1\,1\,2\,1 \end{pmatrix}$
$(\mathbf{B}_{sc\_1/2}, \mathbf{B}_{cc\_2/3})$	$\begin{pmatrix} 7\,1\,1\,1 \\ 3\,1\,1\,2 \end{pmatrix}$	$\begin{pmatrix} 1\,2\,0\,0\,0\,0\,0 \\ 0\,3\,2\,1\,1\,1\,2 \\ 0\,1\,3\,1\,1\,1\,2 \end{pmatrix}$
$(\mathbf{B}_{sc\_2/3}, \mathbf{B}_{cc\_2/3})$	$\begin{pmatrix} 1\,3\,1 \\ 1\,3\,2 \end{pmatrix}$	$\begin{pmatrix} 1\,2\,0\,0\,0\,0\,0 \\ 0\,3\,2\,1\,1\,1\,3 \\ 0\,1\,2\,1\,1\,1\,1 \end{pmatrix}$
$(\mathbf{B}_{sc\_3/4}, \mathbf{B}_{cc\_2/3})$	$\begin{pmatrix} 2\,0\,1\,0 \\ 2\,1\,2\,0 \\ 8\,2\,1\,2 \end{pmatrix}$	$\begin{pmatrix} 1\,2\,0\,0\,0\,0\,0 \\ 0\,3\,1\,1\,1\,1\,1 \\ 0\,1\,3\,1\,1\,2\,2 \end{pmatrix}$
$(\mathbf{B}_{sc\_4/5}, \mathbf{B}_{cc\_2/3})$	$\begin{pmatrix} 1\,1\,1\,1\,0 \\ 1\,1\,1\,0\,1 \\ 1\,1\,0\,1\,0 \\ 1\,0\,0\,0\,1 \end{pmatrix}$	$\begin{pmatrix} 1\,2\,0\,0\,0\,0\,0 \\ 0\,3\,3\,1\,1\,1\,1 \\ 0\,1\,1\,3\,2\,2\,1 \end{pmatrix}$
$(\mathbf{B}_{sc\_1/4}, \mathbf{B}_{cc\_1/2})$	$\begin{pmatrix} 5\,3\,3\,1\,2\,1\,2\,1 \\ 1\,2\,1\,1\,8\,2\,1\,1 \end{pmatrix}$	$\begin{pmatrix} 1\,2\,0\,0\,0 \\ 0\,2\,3\,1\,1 \\ 0\,1\,1\,1\,1 \end{pmatrix}$
$(\mathbf{B}_{sc\_1/3}, \mathbf{B}_{cc\_1/2})$	$\begin{pmatrix} 3\,1\,1\,1\,6\,1 \\ 3\,2\,1\,1\,8\,2 \end{pmatrix}$	$\begin{pmatrix} 1\,2\,0\,0\,0 \\ 0\,3\,1\,1\,1 \\ 0\,1\,1\,1\,2 \end{pmatrix}$
$(\mathbf{B}_{sc\_1/2}, \mathbf{B}_{cc\_1/2})$	$\begin{pmatrix} 1\,1\,6\,2 \\ 1\,1\,2\,2 \end{pmatrix}$	$\begin{pmatrix} 1\,2\,0\,0\,0 \\ 0\,3\,1\,1\,1 \\ 0\,1\,1\,1\,2 \end{pmatrix}$
$(\mathbf{B}_{sc\_2/3}, \mathbf{B}_{cc\_1/2})$	$\begin{pmatrix} 5\,1\,1 \\ 3\,1\,1 \end{pmatrix}$	$\begin{pmatrix} 1\,2\,0\,0\,0 \\ 0\,1\,1\,1\,1 \\ 0\,2\,1\,1\,2 \end{pmatrix}$
$(\mathbf{B}_{sc\_3/4}, \mathbf{B}_{cc\_1/2})$	$\begin{pmatrix} 1\,2\,2\,5 \\ 1\,1\,0\,1 \\ 0\,1\,0\,3 \end{pmatrix}$	$\begin{pmatrix} 1\,2\,0\,0\,0 \\ 0\,2\,1\,1\,1 \\ 0\,1\,1\,1\,2 \end{pmatrix}$
$(\mathbf{B}_{sc\_4/5}, \mathbf{B}_{cc\_1/2})$	$\begin{pmatrix} 1\,1\,1\,1\,0 \\ 1\,1\,1\,0\,1 \\ 1\,1\,0\,1\,0 \\ 1\,0\,0\,0\,1 \end{pmatrix}$	$\begin{pmatrix} 1\,2\,0\,0\,0 \\ 0\,3\,1\,1\,1 \\ 0\,1\,2\,2\,1 \end{pmatrix}$
$(\mathbf{B}_{sc\_1/4}, \mathbf{B}_{cc\_1/3})$	$\begin{pmatrix} 3\,1\,4\,3\,1\,1\,2\,1 \\ 1\,3\,1\,0\,3\,1\,1\,1\,2 \end{pmatrix}$	$\begin{pmatrix} 1\,2\,0\,0\,0\,0\,0 \\ 0\,3\,1\,1\,0\,1\,0 \\ 0\,1\,2\,0\,0\,2\,1 \\ 0\,1\,1\,0\,0\,0\,1 \\ 0\,0\,2\,0\,1\,0\,2 \end{pmatrix}$
$(\mathbf{B}_{sc\_1/3}, \mathbf{B}_{cc\_1/3})$	$\begin{pmatrix} 3\,2\,3\,2\,3\,3 \\ 1\,1\,2\,2\,1\,8 \end{pmatrix}$	$\begin{pmatrix} 1\,2\,0\,0\,0\,0\,0 \\ 0\,3\,2\,1\,1\,2\,1 \\ 0\,0\,1\,0\,2\,0\,2 \\ 0\,2\,1\,0\,0\,1\,1 \\ 0\,1\,2\,0\,0\,0\,0 \end{pmatrix}$
$(\mathbf{B}_{sc\_1/2}, \mathbf{B}_{cc\_1/3})$	$\begin{pmatrix} 3\,1\,3\,1 \\ 2\,1\,7\,1 \end{pmatrix}$	$\begin{pmatrix} 1\,2\,0\,0\,0\,0\,0 \\ 0\,1\,1\,0\,0\,1\,1 \\ 0\,1\,2\,0\,0\,1\,2 \\ 0\,1\,1\,1\,0\,0\,1 \\ 0\,1\,2\,0\,1\,0\,0 \end{pmatrix}$
$(\mathbf{B}_{sc\_2/3}, \mathbf{B}_{cc\_1/3})$	$\begin{pmatrix} 1\,1\,4 \\ 2\,1\,4 \end{pmatrix}$	$\begin{pmatrix} 1\,2\,0\,0\,0\,0\,0 \\ 0\,3\,1\,0\,0\,0\,1 \\ 0\,1\,2\,1\,0\,0\,2 \\ 0\,2\,1\,0\,1\,0\,0 \\ 0\,1\,2\,0\,1\,2\,0 \end{pmatrix}$
$(\mathbf{B}_{sc\_3/4}, \mathbf{B}_{cc\_1/3})$	$\begin{pmatrix} 1\,1\,1\,1 \\ 2\,1\,1\,0 \\ 1\,1\,0\,1 \end{pmatrix}$	$\begin{pmatrix} 1\,2\,0\,0\,0\,0\,0 \\ 0\,3\,1\,0\,1\,1\,0 \\ 0\,1\,1\,0\,1\,1\,0 \\ 0\,2\,1\,0\,0\,0\,1 \\ 0\,1\,2\,1\,0\,0\,1 \end{pmatrix}$
$(\mathbf{B}_{sc\_4/5}, \mathbf{B}_{cc\_1/3})$	$\begin{pmatrix} 1\,1\,1\,1\,0 \\ 1\,1\,1\,0\,1 \\ 1\,1\,0\,1\,0 \\ 1\,0\,0\,0\,1 \end{pmatrix}$	$\begin{pmatrix} 1\,2\,0\,0\,0\,0\,0 \\ 0\,3\,1\,1\,1\,0\,0 \\ 0\,1\,2\,2\,1\,0\,0 \\ 0\,2\,1\,0\,0\,1\,0 \\ 0\,1\,2\,0\,0\,0\,1 \end{pmatrix}$

TABLE 8. *(Continued.)* **Optimized code pairs with parameters of $N = 720$ and $\beta = 0.99$.**

$(\mathbf{B}_{sc\_1/4}, \mathbf{B}_{cc\_1/4})$	$\begin{pmatrix} 3&1&1&1&3&1&2&2 \\ 1&2&1&3&3&1&3&1 \end{pmatrix}$	$\begin{pmatrix} 1&2&0&0&0&0&0&0&0 \\ 0&1&1&0&0&0&1&1&0 \\ 0&1&2&0&0&2&1&0&0 \\ 0&2&1&0&0&0&0&0&1 \\ 0&1&2&0&0&0&0&1&1 \\ 0&2&0&1&0&0&0&0&1 \\ 0&1&1&0&1&0&0&0&0 \end{pmatrix}$
$(\mathbf{B}_{sc\_1/3}, \mathbf{B}_{cc\_1/4})$	$\begin{pmatrix} 3&1&3&3&1&1 \\ 7&2&1&3&1&2 \end{pmatrix}$	$\begin{pmatrix} 1&2&0&0&0&0&0&0&0 \\ 0&3&1&0&0&0&1&1&0 \\ 0&1&2&0&0&0&1&1&0 \\ 0&2&1&1&0&0&0&0&0 \\ 0&1&2&0&0&0&0&0&1 \\ 0&2&1&0&1&0&0&0&2 \\ 0&1&0&0&0&1&0&0&0 \end{pmatrix}$
$(\mathbf{B}_{sc\_1/2}, \mathbf{B}_{cc\_1/4})$	$\begin{pmatrix} 3&1&1&1 \\ 1&2&1&2 \end{pmatrix}$	$\begin{pmatrix} 1&2&0&0&0&0&0&0&0 \\ 0&3&1&1&0&0&0&1&0 \\ 0&0&2&0&0&0&0&2&1 \\ 0&2&0&0&0&0&1&0&0 \\ 0&1&2&0&1&0&0&0&1 \\ 0&2&1&0&0&0&1&0&1 \\ 0&1&1&0&0&1&0&0&0 \end{pmatrix}$
$(\mathbf{B}_{sc\_2/3}, \mathbf{B}_{cc\_1/4})$	$\begin{pmatrix} 2&1&1 \\ 2&1&1 \end{pmatrix}$	$\begin{pmatrix} 1&2&0&0&0&0&0&0&0 \\ 0&3&1&0&1&0&0&0&0 \\ 0&1&2&2&1&0&0&0&0 \\ 0&2&0&0&0&1&0&0&0 \\ 0&1&2&1&0&0&1&0&0 \\ 0&0&1&1&0&0&0&1&0 \\ 0&1&2&0&0&0&0&0&1 \end{pmatrix}$
$(\mathbf{B}_{sc\_3/4}, \mathbf{B}_{cc\_1/4})$	$\begin{pmatrix} 3&1&1&1 \\ 2&1&0&0 \\ 3&0&2&1 \end{pmatrix}$	$\begin{pmatrix} 1&2&0&0&0&0&0&0&0 \\ 0&3&1&0&1&0&0&1&1 \\ 0&1&2&0&0&0&2&1&1 \\ 0&2&1&1&0&0&1&1&1 \\ 0&1&2&0&0&0&0&1&0 \\ 0&2&1&0&0&0&0&0&0 \\ 0&3&2&0&1&2&0&0&2 \end{pmatrix}$
$(\mathbf{B}_{sc\_4/5}, \mathbf{B}_{cc\_1/4})$	$\begin{pmatrix} 1&1&1&1&0 \\ 1&1&1&0&1 \\ 1&1&0&1&0 \\ 1&0&0&0&1 \end{pmatrix}$	$\begin{pmatrix} 1&2&0&0&0&0&0&0&0 \\ 0&3&1&1&1&0&0&0&0 \\ 0&1&2&2&1&0&0&0&0 \\ 0&2&1&0&0&1&0&0&0 \\ 0&1&2&0&0&0&1&0&0 \\ 0&2&1&0&0&0&0&1&0 \\ 0&1&2&0&0&0&0&0&1 \end{pmatrix}$
$(\mathbf{B}_{sc\_1/4}, \mathbf{B}_{cc\_1/5})$	$\begin{pmatrix} 3&1&3&1&2&3&1&1 \\ 1&2&1&3&1&1&1&2 \end{pmatrix}$	$\begin{pmatrix} 1&2&0&0&0&0&0&0&0&0&0 \\ 0&3&1&0&0&0&0&0&1&1 \\ 0&1&2&0&0&0&0&0&1&2 \\ 0&2&1&1&0&0&0&0&0&0 \\ 0&1&2&0&1&0&0&0&0&0 \\ 0&2&1&0&0&1&0&0&0&0 \\ 0&1&2&0&0&0&1&0&0&0 \\ 0&2&1&0&0&0&0&1&0&0 \\ 0&2&2&0&0&0&0&0&1&0 \end{pmatrix}$
$(\mathbf{B}_{sc\_1/3}, \mathbf{B}_{cc\_1/5})$	$\begin{pmatrix} 3&1&1&1&1&3 \\ 3&2&2&1&1&2 \end{pmatrix}$	$\begin{pmatrix} 1&2&0&0&0&0&0&0&0&0&0 \\ 0&3&1&0&0&0&0&0&1&1 \\ 0&1&2&0&0&0&0&0&2&1 \\ 0&2&1&1&0&0&0&0&0&0 \\ 0&1&2&0&1&0&0&0&0&0 \\ 0&2&1&0&0&1&0&0&0&0 \\ 0&1&2&0&0&0&1&0&0&1 \\ 0&2&1&0&0&0&0&1&0&0 \\ 0&1&2&0&0&0&0&0&1&0 \end{pmatrix}$
$(\mathbf{B}_{sc\_1/2}, \mathbf{B}_{cc\_1/5})$	$\begin{pmatrix} 3&1&1&1 \\ 1&2&1&2 \end{pmatrix}$	$\begin{pmatrix} 1&2&0&0&0&0&0&0&0&0&0 \\ 0&3&1&0&0&0&1&0&1&1 \\ 0&2&2&0&0&0&1&1&0&2 \\ 0&2&1&0&0&0&0&1&1&0 \\ 0&1&2&0&0&0&0&0&0&0 \\ 0&2&1&1&0&0&0&0&0&0 \\ 0&1&2&0&1&0&0&0&1&1 \\ 0&2&1&0&0&0&0&2&1&0 \\ 0&1&2&0&0&1&0&0&0&0 \end{pmatrix}$

APPENDIX

Table 8 lists all the proposed code pairs ($\mathbf{B}_{IR4JA}$, $\mathbf{B}_{IAR4JA}$) used in the pro2 method for image transmission with coding rates in $\mathfrak{R}_{sc}$ and $\mathfrak{R}_{cc}$. The block size of the image frame is $N = 720$, and the parameter β is set as 0.99. The sub-matrices which have not the optimal results by GA follow the original forms of $\mathbf{B}_{R4JA}$ or $\mathbf{B}_{AR4JA}$.

TABLE 8. *(Continued.)* **Optimized code pairs with parameters of $N = 720$ and $\beta = 0.99$.**

$(\mathbf{B}_{sc\_2/3}, \mathbf{B}_{cc\_1/5})$	$\begin{pmatrix} 2&2&1 \\ 2&1&1 \end{pmatrix}$	$\begin{pmatrix} 1&2&0&0&0&0&0&0&0&0&0&0 \\ 0&3&1&1&1&0&0&0&0&0&0 \\ 0&1&2&2&1&0&0&0&0&0&0 \\ 0&2&1&0&0&1&0&0&0&0&0 \\ 0&1&2&0&0&0&1&0&0&0&0 \\ 0&2&1&0&0&0&0&1&0&0&0 \\ 0&1&2&0&0&0&0&0&1&0&0 \\ 0&2&1&0&0&0&0&0&0&1&0 \\ 0&1&2&0&0&0&0&0&0&0&1 \end{pmatrix}$
$(\mathbf{B}_{sc\_3/4}, \mathbf{B}_{cc\_1/5})$	$\begin{pmatrix} 1&1&1&1 \\ 2&1&1&0 \\ 1&1&0&1 \end{pmatrix}$	$\begin{pmatrix} 1&2&0&0&0&0&0&0&0&0&0&0 \\ 0&3&1&1&1&0&0&0&0&0&0 \\ 0&1&2&2&1&0&0&0&0&0&0 \\ 0&2&1&0&0&1&0&0&0&0&0 \\ 0&1&2&0&0&0&1&0&0&0&0 \\ 0&2&1&0&0&0&0&1&0&0&0 \\ 0&1&2&0&0&0&0&0&1&0&0 \\ 0&2&1&0&0&0&0&0&0&1&0 \\ 0&1&2&0&0&0&0&0&0&0&1 \end{pmatrix}$
$(\mathbf{B}_{sc\_4/5}, \mathbf{B}_{cc\_1/5})$	$\begin{pmatrix} 1&1&1&1&0 \\ 1&1&1&0&1 \\ 1&1&0&1&0 \\ 1&0&0&0&1 \end{pmatrix}$	$\begin{pmatrix} 1&2&0&0&0&0&0&0&0&0&0&0 \\ 0&3&1&1&1&0&0&0&0&0&0 \\ 0&1&2&2&1&0&0&0&0&0&0 \\ 0&2&1&0&0&1&0&0&0&0&0 \\ 0&1&2&0&0&0&1&0&0&0&0 \\ 0&2&1&0&0&0&0&1&0&0&0 \\ 0&1&2&0&0&0&0&0&1&0&0 \\ 0&2&1&0&0&0&0&0&0&1&0 \\ 0&1&2&0&0&0&0&0&0&0&1 \end{pmatrix}$

REFERENCES

[1] C. Zhu, V. C. M. Leung, J. J. P. C. Rodrigues, L. Shu, L. Wang, and H. Zhou, "Social sensor cloud: Framework, greenness, issues, and outlook," *IEEE Netw.*, vol. 32, no. 5, pp. 100–105, Sep./Oct. 2018.

[2] *NB-IoT: A Sustainable Tech*, Ericsson, Stockholm, Sweden, 2016.

[3] C. Zhu, J. J. P. C. Rodrigues, V. C. M. Leung, L. Shu, and L. T. Yang, "Trust-based communication for the industrial Internet of Things," *IEEE Commun. Mag.*, vol. 56, no. 2, pp. 16–22, Feb. 2018.

[4] C. Zhu, L. Shu, V. C. M. Leung, S. Guo, Y. Zhang, and L. T. Yang, "Secure multimedia big data in trust-assisted sensor-cloud for smart city," *IEEE Commun. Mag.*, vol. 55, no. 12, pp. 24–30, Dec. 2017.

[5] *Evolved Universal Terrestrial Radio Access (E-UTRA) and Evolved Universal Terrestrial Radio Access Network (E-UTRAN); Physical Layer Procedures, Version 13.3.0*, document 3GPP TS36.213, Sep. 2016.

[6] F. N. Hidayah and K. Anwar, "Low density generator matrix (LDGM)-based Raptor codes for single carrier Internet of Things (SC-IoT)," in *Proc. Int. Conf. Signals Syst. (ICSigSys)*, May 2017, pp. 24–28.

[7] M. Ejaz, K. Khurshid, Z. Abbas, M. A. Aizaz, and A. Nawaz, "A novel image encoding and communication technique of B/W images for IOT, robotics and drones using (15, 11) Reed Solomon scheme," in *Proc. int. Conf. Adv. Sci. Eng. Tech. (ASET)*, Apr. 2018, pp. 1–6.

[8] I. A. Shah, F. A. Malik, and S. A. Ahmad, "Enhancing security in IoT based Home automation using Reed Solomon Codes," in *Proc. Int. Conf. Wireless Commun. Signals Process. Netw. (WiSPNET)*, Mar. 2016, pp. 1639–1642.

[9] T. J. Richardson and R. L. Urbanke, "Efficient encoding of low-density parity-check codes," *IEEE Trans. Inf. Theory*, vol. 47, no. 2, pp. 638–656, Feb. 2001.

[10] J. L. Massey, "Joint source and channel coding," in *Communications Systems and Random Process Theory*, vol. 11. Dordrecht, The Netherlands: Sijthoff and Nordhoff, 1978, pp. 279–293.

[11] L. Pu, Z. Wu, A. Bilgin, M. W. Marcellin, and B. Vasic, "LDPC-based iterative joint source-channel decoding for JPEG2000," *IEEE Trans. Image Process.*, vol. 16, no. 2, pp. 577–581, Feb. 2007.

[12] M. Fresia, F. Pérez-Cruz, H. V. Poor, and S. Verdú, "Joint source and channel coding," *IEEE Signal Process. Mag.*, vol. 27, no. 6, pp. 104–113, Nov. 2010.
[13] J. He, L. Wang, and P. Chen, "A joint source and channel coding scheme base on simple protograph structured codes," in *Proc. Int. Symp. Commun. Inf. Technol. (ISCIT)*, Oct. 2012, pp. 65–69.
[14] L. Xu, H. Wu, J. He, and L. Wang, "Unequal error protection for radiography image transmission using protograph double LDPC codes," in *Proc. Int. Symp. Wireless Telecommun. (WTS)*, Jun. 2013, pp. 1–5.
[15] H. Wu, L. Wang, S. Hong, and J. He, "Performance of joint source-channel coding based on protograph LDPC codes over Rayleigh fading channels," *IEEE Commun. Lett.*, vol. 18, no. 4, pp. 652–655, Apr. 2014.
[16] Q. Chen, L. Wang, and S. Hong, "An image pre-processing approach for JSCC scheme based on double protograph LDPC codes," in *Proc. Int. Symp. Commun. Inf. Technol. (ISCIT)*, Sep. 2016, pp. 109–112.
[17] H. V. B. Neto and W. Henkel, "Multi-edge optimization of low-density parity-check codes for joint source-channel coding," in *Proc. Int. ITG Conf. Syst., Commun. Coding*, Jan. 2013, pp. 1–6.
[18] S. Hong, Q. Chen, and L. Wang, "Performance analysis and optimisation for edge connection of JSCC system based on double protograph LDPC codes," *IET Commun.*, vol. 12, no. 2, pp. 214–219, Feb. 2018.
[19] C. Chen, L. Wang, and Z. Xiong, "Matching criterion between source statistics and source coding rate," *IEEE Commun. Lett.*, vol. 19, no. 9, pp. 1504–1507, Sep. 2015.
[20] Q. Chen, L. Wang, S. Hong, and Z. Xiong, "Performance improvement of JSCC scheme through redesigning channel code," *IEEE Commun. Lett.*, vol. 20, no. 6, pp. 1088–1091, Jun. 2016.
[21] C. Chen, L. Wang, and S. Liu, "The design of protograph LDPC codes as source codes in a JSCC system," *IEEE Commun. Lett.*, vol. 22, no. 4, pp. 672–675, Apr. 2018.
[22] C. Chen, L. Wang, and F. C. M. Lau, "Joint optimization of protograph LDPC code pair for joint source and channel coding," *IEEE Trans. Commun.*, vol. 66, no. 8, pp. 3255–3267, Aug. 2018.
[23] L. Deng, Z. Shi, S. Zhang, R. Tang, and L. Gan, "Effective adaptive rate allocation for DP-LDPC image transmission system based on source and channel characteristics," in *Proc. Int. Conf. Commun. Technol. (ICCT)*, Chengdu, China, Oct. 2017, pp. 539–544.
[24] J. Thorpe, "Low density parity check (LDPC) codes constructed from protographs," Nat. Aeronaut. Space Admin., Washington, DC, USA, IPN Prog. Rep. 42-154, Aug. 2003.
[25] D. Divsalar, S. Dolinar, C. Jones, and K. Andrews, "Capacity approaching protograph codes," *IEEE J. Sel. Areas Commun.*, vol. 27, no. 6, pp. 876–888, Aug. 2009.
[26] H. Uchikawa, "Design of non-precoded protograph-based LDPC codes," in *Proc. Symp. Inf. Theory (ISIT)*, Jun. 2014, pp. 2779–2783.
[27] T. Van Nguyen, A. Nosratinia, and D. Divsalar, "The design of rate-compatible protograph LDPC codes," *IEEE Trans. Commun.*, vol. 60, no. 10, pp. 2841–2850, Oct. 2012.
[28] X.-Y. Hu, E. Eleftheriou, and D. M. Arnold, "Regular and irregular progressive edge-growth tanner graphs," *IEEE Trans. Inf. Theory*, vol. 51, no. 1, pp. 386–398, Jan. 2005.

LI DENG received the B.Sc. and M.Sc. degrees from Southwest University, Chongqing, China, in 2005 and 2008, respectively. She is currently pursuing the Ph.D. degree with the National Key Laboratory of Science and Technology on Communications, University of Electronic Science and Technology of China. She is currently an Associate Professor with the School of Electronic Information and Automation, Guilin University of Aerospace Technology, China. Her research interests include information and coding theory, protograph LDPC codes, and wireless image communication.

ZHIPING SHI received the master's and Ph.D. degrees from Southwest Jiaotong University, Chengdu, China, in 1998 and 2005, respectively. She held a Post-Doctoral position at the University of Electronic Science and Technology of China (UESTC), from 2005 to 2007. She was a Visiting Scholar with Lehigh University, Bethlehem, PA, USA, from 2009 to 2010. In 2007, she joined the School of Communication and Information, UESTC, where she is currently a Professor with the National Key Lab of Communications. Her research interests include coding theory, cognitive radio, and wireless communications.

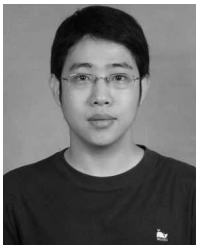

OUXUN LI received the B.Sc. and M.Sc. degrees from Chongqing University, Chongqing, China, in 2005 and 2009, respectively. He is currently pursuing the Ph.D. degree with the College of Automation Engineering, Nanjing University of Aeronautics and Astronautics, Nanjing, China. He is also a Lecturer with the School of Electronic Information and Automation, Guilin University of Aerospace Technology, China. His research interests include navigation guidance and control, fuzzy sliding mode control, and type-2 fuzzy logic control.

JIANBO JI received the B.Sc. degree in electrical engineering from Jiangxi Normal University, Nanchang, China, in 1997, the M.Sc. degree in communication engineering from the Guilin University of Electronic Technology, Guilin, China, in 2004, and the Ph.D. degree in signal and information processing form Shanghai Jiao Tong University, Shanghai, China, in 2016. He has published 17 papers in IEEE journals and conferences. His research interests include communication theory and its applications in practical communication systems, cooperative diversity, and cognitive radio techniques.